Inorganic Chemistry

Article

pubs.acs.org/IC

New Layered Tin(II) Thiophosphates $ASnPS_4$ (A = K, Rb, Cs): Synthesis, Structure, Glass Formation, and the Modulated $CsSnPS_4$

Santanu Banerjee,[†] Christos D. Malliakas,[†] and Mercouri G. Kanatzidis*[,†,‡]

[†]Department of Chemistry, Northwestern University, Evanston, Illinois 60208, United States

[‡]Materials Science Division, Argonne National Laboratory, Argonne, Illinois 60439, United States

Supporting Information

ABSTRACT: The layered compounds $KSnPS_4$ (**1**), $RbSnPS_4$ (**2**), and $CsSnPS_4$ (**3**) were synthesized using the chalcophosphate flux technique at high temperature and are rare examples of divalent Sn(II) thiophosphates. Orange polyhedral crystals of compound **1** crystallize in the monoclinic space group $P2_1/c$ with a = 6.6673(13) Å, b = 11.9697(24) Å, c = 8.7604(18), and β=127.347(8)° in a 2-dimensional layered structure. Compound **2** is isostructural to **1**. Yellow block shaped crystals of compound **3** crystallize in the monoclinic superspace group $P2_1(\alpha\beta0)0$ with a commensurate q-vector at 1/4a* + 1/4c* with a = 18.0477(14) Å, b = 6.2021(5) Å, and c = 6.8415(5) Å. The structure of all three compounds contains SnS_3 pyramids, which is an extremely rare solid state chalcogenide coordination environment. All three compounds are semiconductors having well-defined band-gaps between 2.0 and 2.2 eV. The compounds are congruently melting and can be obtained as glasses by rapid quenching of the melt, which subsequently crystallize upon heating.

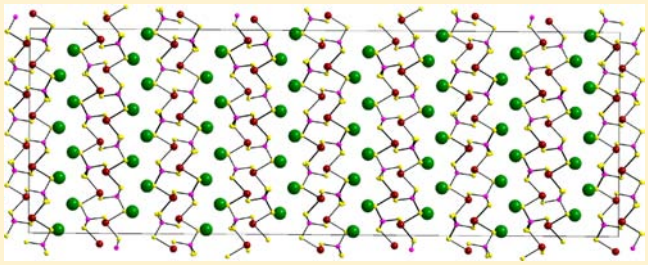

INTRODUCTION

The use of a polychalcogenide flux as a reaction medium in solid state syntheses has resulted in numerous ternary and quaternary metal chalcophosphate phases with wide structural diversity as well as unique materials properties. The chalcophosphates are typically medium to wide band gap semiconductors having very interesting physical properties like ferroelectricity,[1−9] photoconductivity,[10] electro-optic,[11] and nonlinear optical[12−15] properties. All chalcophosphate anions are potential ligands to metal ions for building finite or extended structures and, in principle, can produce more diverse families of compounds compared to their more limited oxophosphate $[P_xO_y]^{z-}$ counterparts. This is attributed to the unique ability of the molecular anions, $[P_xQ_y]^{z-}$, to oxidatively couple through Q-Q bonds to form larger structures having $[P\text{-}Q\text{-}Q\text{-}P]_n$ linkages. In the literature, there exist examples of chalcophosphate phases isolated using the molten flux technique,[16] which are usually ternary (M/P/Q) or quaternary (A/M/P/Q) compounds, where A = alkali metal, M = nonalkali metal, and Q = chalcogen (S, Se, Te). The anionic thiophosphate $[P_xS_y]^{n-}$ groups are known to bind to main group metal ions,[17−19] transition metal ions,[19−25] lanthanides,[19,26−44] and actinides[45−47] to form a variety of ternary and quaternary compounds. Tin chalcogenides are well-known to assume interesting layered structures, in which tin can adopt flexible coordination geometries such as tetrahedral, octahedral, and trigonal bipyramidal.[48−50] Investigation of the A/Sn/P/S system is particularly interesting as there exists the Pb compound, $KPbPS_4$,[51] which has a layered structure and is isostructural to $KEuPS_4$.[43] Tin can bind to various thiophosphate anions like $[PS_4]^{3-}$, $[P_2S_7]^{4-}$, $[P_2S_9]^{2-}$,[20] $[P_2S_6]^{2-}$,[21] $[P_2S_6]^{4-}$[52], and so forth. Both divalent and tetravalent tin thiophosphates such as $Sn_2P_2S_6$,[53,54] SnP_2S_6,[55] $Sn_2P_2S_8$[56] are well-known for their interesting properties. Although there exists a great number of tetravalent tin thiophosphates in the literature, examples of quaternary divalent tin thiophosphate compounds are rare.[57−62] We report here the synthesis, structure, characterization, and glass formation properties of alkali metal salts of a new family of quaternary divalent tin thiophosphates, $ASnPS_4$ [A = K(**1**), Rb (**2**), and the modulated Cs (**3**)].

EXPERIMENTAL SECTION

Reagents. The reagents employed in this work were used as obtained: K metal, Aldrich Chemical Co., Milwaukee, WI; Rb, Cs metal, analytical reagent, Strem Chemicals, Newburyport, MA; red phosphorus powder, −100 mesh, Morton Thiokol, Inc., Danvers, MA; S, 99.9999%, Noranda Advanced Materials, Quebec, Canada; *N,N*-dimethylformamide (DMF), ACS reagent grade, Mallinckrodt Baker Inc., Paris, KY; diethyl ether, ACS reagent grade, anhydrous, Columbus Chemical Industries, Columbus, WI. K_2S, Rb_2S, and Cs_2S starting materials were prepared by reacting stoichiometric amounts of the elements in liquid ammonia following the procedure reported elsewhere.[63,64]

Synthesis. *Preparation of $KSnPS_4$ (1).* In a nitrogen-filled glovebox, K_2S, Sn, red P, and S were loaded in a 1:2.5:2:9 ratio in a 9 mm fused silica tube, which was then sealed under vacuum (<10^{-4} mbar). The reaction mixture was heated at 900 °C for 72 h followed

Received: July 5, 2012
Published: October 9, 2012

   dx.doi.org/10.1021/ic301456m | *Inorg. Chem.* 2012, 51, 11562−11573

by cooling to 300 °C in 120 h and finally to room temperature in 3 h. The solidified yellow-orange colored melt was then taken out of the tube and washed with degassed *N*,*N*-dimethylformamide. Yellow-orange colored polyhedral crystals (yield ∼80% based on Sn) were isolated after drying with ether. A small amount of orange flakes of tin sulfide (SnS_2) was identified as a side product. Elemental analysis using SEM-EDS showed the approximate composition of a single crystal is K:Sn:P:S = 1:1:1:4.

*Preparation of $RbSnPS_4$ (**2**).* In a nitrogen-filled glovebox, Rb_2S, Sn, red P, and S were loaded in a 1:2.5:2:9 ratio in a 9 mm fused silica tube, which was then sealed under vacuum ($<10^{-4}$ mbar). The reaction mixture was heated at 900 °C for 72 h followed by cooling to 300 °C in 120 h and finally to room temperature in 3 h. The solidified yellow-orange colored melt was then taken out of the tube and washed with degassed *N*,*N*-dimethylformamide. Yellow-orange colored polyhedral crystals (yield ∼80%) were isolated after drying with ether. A small amount of orange flakes of tin sulfide (SnS_2) was identified as a side product. Elemental analysis using SEM-EDS showed the approximate composition of a single crystal is Rb:Sn:P:S = 1:1:1:4.

*Preparation of $CsSnPS_4$ (**3**).* In a nitrogen-filled glovebox, Cs_2S, Sn, red P, and S were loaded in a 1:2.5:2:9 ratio in a 9 mm fused silica tube, which was then sealed under vacuum ($<10^{-4}$ mbar). The reaction mixture was heated at 900 °C for 72 h followed by cooling to 300 °C in 120 h and finally to room temperature in 3 h. The solidified yellow-orange colored melt was then taken out of the tube and washed with degassed *N*,*N*-dimethylformamide. Yellow-orange colored polyhedral crystals (yield ∼80%) were isolated after drying with ether. A small amount of orange flakes of tin sulfide (SnS_2) was identified as a side product. Elemental analysis using SEM-EDS showed the approximate composition of a single crystal is Cs:Sn:P:S = 1:1:1:4.

Physical Measurements. *Powder X-ray Diffraction.* Phase-purity X-ray diffraction analyses were performed using a silicon calibrated CPS 120 INEL powder X-ray diffractometer (Cu Kα graphite monochromatized radiation) operating at 40 kV and 20 mA, equipped with a position-sensitive detector with flat sample geometry.

Scanning Electron Microscopy. Scanning electron microscopy (SEM) semiquantitative analyses and morphology images of the compounds were obtained with a JEOL JSM-35C scanning electron microscope (SEM) equipped with a Tracor Northern EDS detector.

Solid-State UV−vis Spectroscopy. Optical diffuse reflectance measurements were performed at room temperature using a Shimadzu UV-3101 PC double-beam, double-monochromator spectrophotometer operating in the 200−2500 nm region, using $BaSO_4$ as a standard. The generated reflectance-versus-wavelength data were used to estimate the band gap of the material by converting reflectance to absorption data according to the Kubelka−Munk equation: $\alpha/S = (1 - R)^2/(2R)$,[65−67] where R is the reflectance and α and S are the absorption and scattering coefficients, respectively.

Raman Spectroscopy. Raman spectra were recorded on a DeltaNu Advantage NIR Raman spectrograph equipped with a charge-coupled device (CCD) camera detector using 785 nm radiation from a diode laser for excitation. The laser power at the sample was estimated to be maximum ∼60 mW and the focused laser beam diameter was ∼35 μm.

Infrared Spectroscopy. FT-IR spectra were recorded on pure crystalline samples by placing them in the sample holder. The spectra were recorded in the far-IR (600−100 cm^{-1}) and mid-IR (500−4000 cm^{-1}) regions with 4 cm^{-1} resolution using a Nicolet 740 FT-IR spectrometer equipped with a TGS/PE detector and silicon beam splitter.

Differential Thermal Analysis. Differential thermal analysis (DTA) experiments were performed on a Shimadzu DTA-50 thermal analyzer, using Al_2O_3 as the standard. The sample was heated to 800 at 10 °C min^{-1}, and after 1 min, was cooled at a rate of −10 °C min^{-1} to 50 °C. The residues of the DTA experiments were examined by powder X-ray diffraction. The melting and crystallization points were measured at the minimum of the endothermic peak and the maximum of the exothermic peak, respectively.

Solid State Nuclear Magnetic Resonance (NMR) Spectroscopy. ^{31}P magic angle spinning (MAS) NMR spectra were recorded on a Varian Mercury 400 spectrometer and referenced to $NH_4H_2PO_4$ (δ 0.8). The delay time between scans was 120 s. A total of 128 scans were collected for compounds **1** and **3**.

X-ray Crystallography. Intensity data for $KSnPS_4$ (**1**) and $CsSnPS_4$ (**3**) were collected at 100 K on a STOE IPDS 2T diffractometer with Mo Kα radiation operating at 50 kV and 40 mA with a 34 cm diameter imaging plate (Compound **2** is isostructural to **1**). Individual frames were collected with a 5 min exposure time and a 1° ω rotation. The X-AREA, X-RED, and X-SHAPE software packages[68] were used for data extraction, integration, and analytical absorption corrections. The SHELXTL software package[69,70] was used to solve and refine the structure of **1**. A pseudomerohedral twin law [-1 0 0 0 -1 0 2 0 1] was used with a refined twin fraction of 53.0(1)%. The most satisfactory refinement was obtained with the space group $P2_1/c$ for compound **1**. The parameters for data collection, details of the structural refinement, fractional atomic coordinates, atomic displacement parameters, and selected bond distances and angles for **1** are given in Tables 1 to 5, respectively.

Table 1. Crystal Data and Structure Refinement for $KSnPS_4$[a]

empirical formula	$KSnPS_4$
formula weight	317.00
temperature	100.0(3) K
wavelength	0.71073 Å
crystal system	monoclinic
space group	$P2_1/c$
unit cell dimensions	a = 6.6763(8) Å, α = 90.00°
	b = 11.9806(11) Å, β = 127.347(8)°
	c = 10.9970(14) Å, γ = 90.00°
volume	699.27(14) Å^3
Z	4
density (calculated)	3.011 g/cm^3
absorption coefficient	5.548 mm^{-1}
F(000)	592
crystal size	0.14 × 0.03 × 0.02 mm^3
θ range for data collection	3.84 to 26.50°
index ranges	$-8 \le h \le 8$, $-14 \le k \le 14$, $-13 \le l \le 13$
reflections collected	4924
independent reflections	1390 [R_{int} = 0.0356]
completeness to θ = 26.50°	96.1%
refinement method	full-matrix least-squares on F^2
data/restraints/parameters	1390/0/66
goodness-of-fit	1.094
final R indices [$>2\sigma(I)$]	R_{obs} = 0.0199, wR_{obs} = 0.0478
R indices [all data]	R_{all} = 0.0215, wR_{all} = 0.0482
rxtinction coefficient	0.0062(5)
largest diff. peak and hole	0.841 and −0.918 e·Å^{-3}

[a] $R = \sum||F_o| - |F_c||/\sum|F_o|$, $wR = \{\sum[w(|F_o|^2 - |F_c|^2)^2]/\sum[w(|F_o|^4)]\}^{1/2}$ and $w = 1/[\sigma^2(F_o^2) + (0.0306P)^2]$ where $P = (F_o^2 + 2F_c^2)/3$.

Refinement Procedure for the Modulated Structure of Compound 3. The positional distortion of a given atomic parameter x_4 in the subcell was expressed by a periodic modulation function $p(x_4)$ in the form of a Fourier expansion:

$$p(k + x_4) = \sum_{n=1}^{m} A_{sn} \sin[2\pi\bar{q}_n(k + x_4)] + \sum_{n=1}^{m} A_{cn} \cos[2\pi\bar{q}_n(k + x_4)]$$

where A_{sn} is the sinusoidal coefficient of the given Fourier term, A_{cn} the cosine coefficient, $n(=2)$ the number of modulation waves used for the refinement, k the lattice translation, and $\bar{q}_n = \sum_{i=1}^{d} \alpha_{ni}q_i$, where α_{ni} are integer numbers for the linear combination of the commensurate modulation vectors q_i.

dx.doi.org/10.1021/ic301456m | *Inorg. Chem.* 2012, 51, 11562−11573

Table 2. Atomic Coordinates (×10⁴) and Equivalent Isotropic Displacement Parameters (Å² × 10³) for $KSnPS_4$ at 100.0(3) K with Estimated Standard Deviations in Parentheses

label	x	y	z	occupancy	U_{eq}[a]
Sn	6926(1)	3681(1)	3852(1)	1	5(1)
K	1096(2)	978(2)	3711(2)	1	11(1)
P	3559(2)	1604(1)	1287(2)	1	3(1)
S(1)	5299(2)	464(2)	3041(2)	1	7(1)
S(2)	1369(2)	4228(1)	4237(2)	1	5(1)
S(3)	6242(2)	2526(2)	1421(2)	1	6(1)
S(4)	1364(2)	2642(2)	1450(2)	1	6(1)

[a] U_{eq} is defined as one-third of the trace of the orthogonalized U_{ij} tensor.

Table 3. Anisotropic Displacement Parameters (Å² × 10³) for $KPSnS_4$ at 100.0(3) K with Estimated Standard Deviations in Parentheses[a]

label	U_{11}	U_{22}	U_{33}	U_{12}	U_{13}	U_{23}
Sn	6(1)	4(1)	4(1)	0(1)	3(1)	0(1)
K	11(1)	14(1)	8(1)	1(1)	6(1)	0(1)
P	3(1)	3(1)	2(1)	−1(1)	2(1)	−1(1)
S(1)	8(1)	7(1)	3(1)	0(1)	1(1)	1(1)
S(2)	5(1)	8(1)	2(1)	0(1)	2(1)	0(1)
S(3)	6(1)	7(1)	10(1)	−3(1)	6(1)	−2(1)
S(4)	5(1)	6(1)	10(1)	−1(1)	6(1)	−2(1)

[a] The anisotropic displacement factor exponent takes the form: $-2\pi^2[h^2a^{*2}U_{11} + ... + 2hka^*b^*U_{12}]$.

Table 4. Bond Lengths [Å] for $KPSnS_4$ at 100.0(3) K with Estimated Standard Deviations in Parentheses[a]

label	distances	label	distances
Sn−S(1)#1	2.7115(13)	P−S(3)	2.0316(16)
Sn−S(3)	2.7912(13)	P−S(1)	2.0537(17)
Sn−S(2)#2	2.8082(13)	P−S(2)#7	2.0534(16)
K−S(3)#3	3.2218(17)	P−K#7	3.6694(17)
K−S(4)	3.2756(18)	S(1)−Sn#8	2.7115(13)
K−S(1)#4	3.3327(17)	S(1)−K#4	3.3327(17)
K−S(2)#5	3.3373(16)	S(1)−K#2	3.5266(17)
K−S(4)#6	3.3440(17)	S(2)−P#6	2.0534(16)
K−S(1)	3.3625(16)	S(2)−Sn#3	2.8082(12)
K−S(3)#6	3.3875(17)	S(2)−K#9	3.3373(16)
K−S(1)#3	3.5266(17)	S(3)−K#2	3.2218(17)
K−P#6	3.6694(17)	S(3)−K#7	3.3875(17)
P−S(4)	2.0115(15)	S(4)−K#7	3.3440(17)

[a] Symmetry transformations used to generate equivalent atoms: (1) −x+1,y+1/2,−z+1/2 (2) x+1,y,z (3) x−1,y,z (4) −x+1,−y,−z+1 (5) −x,y−1/2,−z+1/2 (6) x,−y+1/2,z+1/2 (7) x,−y+1/2,z−1/2 (8) −x+1,y−1/2,−z+1/2 (9) −x,y+1/2,−z+1/2 (10) −x,−y,−z+1.

Table 5. Bond Angles [deg] for $KPSnS_4$ at 100.0(3) K with Estimated Standard Deviations in Parentheses[a]

label	angles	label	angles
S(1)#1−Sn−S(3)	87.73(4)	S(4)−K−P#6	84.27(4)
S(1)#1−Sn−S(2)#2	88.19(3)	S(1)#4−K−P#6	83.57(4)
S(3)−Sn−S(2)#2	78.71(4)	S(2)#5−K−P#6	166.30(5)
S(3)#3−K−S(4)	63.17(4)	S(4)#6−K−P#6	32.92(3)
S(3)#3−K−S(1)#4	150.02(4)	S(1)−K−P#6	105.71(4)
S(4)−K−S(1)#4	142.43(4)	S(3)#6−K−P#6	33.16(3)
S(3)#3−K−S(2)#5	86.14(4)	S(1)#3−K−P#6	102.72(4)
S(4)−K−S(2)#5	82.35(4)	S(3)#3−K−K#10	103.44(4)
S(1)#4−K−S(2)#5	108.98(5)	S(4)−K−K#10	166.61(5)
S(3)#3−K−S(4)#6	84.18(4)	S(1)#4−K−K#10	50.30(3)
S(4)−K−S(4)#6	112.65(4)	S(2)#5−K−K#10	97.25(5)
S(1)#4−K−S(4)#6	71.44(4)	S(4)#6−K−K#10	63.58(3)
S(2)#5−K−S(4)#6	155.62(4)	S(1)−K−K#10	131.97(5)
S(3)#3−K−S(1)	120.76(5)	S(3)#6−K−K#10	105.21(4)
S(4)−K−S(1)	60.52(4)	S(1)#3−K−K#10	46.65(3)
S(1)#4−K−S(1)	89.07(4)	P#6−K−K#10	95.08(4)
S(2)#5−K−S(1)	69.97(4)	S(3)#3−K−K#4	164.85(5)
S(4)#6−K−S(1)	133.79(4)	S(4)−K−K#4	101.93(4)
S(3)#3−K−S(3)#6	112.68(4)	S(1)#4−K−K#4	44.78(3)
S(4)−K−S(3)#6	81.51(4)	S(2)#5−K−K#4	89.19(4)
S(1)#4−K−S(3)#6	69.14(4)	S(4)#6−K−K#4	105.39(4)
S(2)#5−K−S(3)#6	145.70(4)	S(1)−K−K#4	44.28(3)
S(4)#6−K−S(3)#6	58.30(4)	S(3)#6−K−K#4	65.03(3)
S(1)−K−S(3)#6	75.74(4)	S(1)#3−K−K#4	134.69(5)
S(3)#3−K−S(1)#3	58.75(4)	P#6−K−K#4	96.46(4)
S(4)−K−S(1)#3	120.40(4)	K#10−K−K#4	91.44(4)
S(1)#4−K−S(1)#3	96.95(4)	S(4)−P−S(3)	108.39(8)
S(2)#5−K−S(1)#3	81.69(4)	S(4)−P−S(1)	110.78(7)
S(4)#6−K−S(1)#3	74.14(3)	S(3)−P−S(1)	108.76(6)
S(1)−K−S(1)#3	151.43(6)	S(4)−P−S(2)#7	109.06(7)
S(3)#6−K−S(1)#3	132.44(4)	S(3)−P−S(2)#7	110.66(6)
S(3)#3−K−P#6	85.20(4)	S(1)−P−S(2)#7	109.18(7)
S(4)−P−K#7	64.62(5)	K−S(1)−K#2	151.43(6)
S(3)−P−K#7	65.78(5)	P#6−S(2)−Sn#3	92.03(5)
S(1)−P−K#7	169.50(6)	P#6−S(2)−K#9	167.09(6)
S(2)#7−P−K#7	81.31(5)	Sn#3−S(2)−K#9	98.45(4)
P−S(1)−Sn#8	93.92(5)	P−S(3)−Sn	87.93(5)
P−S(1)−K#4	168.78(6)	P−S(3)−K#2	99.70(6)
Sn#8−S(1)−K#4	96.74(4)	Sn−S(3)−K#2	91.96(4)
P−S(1)−K	90.71(5)	P−S(3)−K#7	81.06(5)
Sn#8−S(1)−K	99.85(4)	Sn−S(3)−K#7	93.98(4)
K#4−S(1)−K	90.93(4)	K#2−S(3)−K#7	174.03(5)
P−S(1)−K#2	90.23(5)	P−S(4)−K	94.00(6)
Sn#8−S(1)−K#2	108.57(4)	P−S(4)−K#7	82.47(5)
K#4−S(1)−K#2	83.05(4)	K−S(4)−K#7	170.70(5)

[a] Symmetry transformations used to generate equivalent atoms: (1) −x+1,y+1/2,−z+1/2 (2) x+1,y,z (3) x−1,y,z (4) −x+1,−y,−z+1 (5) −x,y−1/2,−z+1/2 (6) x,−y+1/2,z+1/2 (7) x,−y+1/2,z−1/2 (8) −x+1,y−1/2,−z+1/2 (9) −x,y+1/2,−z+1/2 (10) −x,−y,−z+1.

The length determination and refinement of the q-vectors was performed with the Peaklist 1.06 software part of the X-Area suite[68] using a least-squares refinement algorithm. The Jana2006 software was used for the structure refinement.[71] Satellite reflections of two orders were observed and used for the refinement. A double modulation wave for the position of the atoms was used. Only the symmetry allowed Fourier terms (A_{sn} and A_{cn}) were refined. More specifically, the sinusoidal coefficients in all directions for the positional (*x*, *y*, and *z*) parameters were freely refined, and the corresponding cosine coefficient values were induced by symmetry. Additionally, a pseudomerohedral twin law [-1 0 0 0 1 0 0 0 1] was used with a refined twin fraction of 50.0(2)%. The crystal structure data and refinement details for **3** are listed in Tables 6 and 7.

Experimental Details for PDF Experiment. Crystalline and glassy $KSnPS_4$ were packed in Kapton capillaries (1 mm diameter), and diffraction data were collected at 100 K using the rapid acquisition pair distribution function (RA-PDF) technique.[72] Data were collected using a Perkin-Elmer a-Si detector and ∼90 keV energy X-rays (λ = 0.13702 Å) at the 11-ID-B beamline at the Advanced Photon Source. To improve counting statistics, 150 frames of 3 s each were collected. The data were combined and integrated using the program FIT2D.[73]

dx.doi.org/10.1021/ic301456m | Inorg. Chem. 2012, 51, 11562−11573

Table 6. Crystal Data and Structure Refinement for $CsSnPS_4$[a]

empirical formula	$CsSnPS_4$
formula weight	410.8
temperature	100.0(3) K
wavelength	0.71073 Å
crystal system	monoclinic
space group	$P2_1/m(\alpha 0\gamma)0s$
unit cell dimensions	a = 6.2031(5) Å, α = 90°
	b = 6.8416(5) Å, β = 90°
	c = 18.0468(14) Å, γ = 90°
q-vector(1)	1/4a* + 1/4c*
volume	765.89(10) Å^3
Z	4
density (calculated)	3.5617 g/cm^3
absorption coefficient	9.207 mm^{-1}
F(000)	736
crystal size	0.17 × 0.10 × 0.04 mm^3
θ range for data collection	3.96 to 29.21°
index ranges	$-8 \le h \le 9$, $-9 \le k \le 9$, $-24 \le l \le 25$, $-2 \le m \le 2$
reflections collected	34902 (7234 main +27668 satellites)
independent reflections	9352 (2233 main +7119 satellites) [R_{int} = 0.0771]
completeness to θ = 29.21°	99%
refinement method	full-matrix least-squares on F^2
data/restraints/parameters	9352/0/139
Goodness-of-fit on F^2	1.45
final R indices [$I > 3\sigma(I)$]	R_{obs} = 0.0618, wR_{obs} = 0.1349
R indices (all data)	R_{all} = 0.1100, wR_{all} = 0.1491
final R main indices [$I > 3\sigma(I)$]	R_{obs} = 0.0396, wR_{obs} = 0.0868
R main indices (all data)	R_{all} = 0.0558, wR_{all} = 0.0912
final R 1st order satellites [$I > 3\sigma(I)$]	R_{obs} = 0.0785, wR_{obs} = 0.1687
R 1st order satellites (all data)	R_{all} = 0.1482, wR_{all} = 0.1842
final R 2nd order satellites [$I > 3\sigma(I)$]	R_{obs} = 0.1098, wR_{obs} = 0.2265
R 2nd order satellites (all data)	R_{all} = 0.1811, wR_{all} = 0.2600
extinction coefficient	400(30)
T_{min} and T_{max} coefficients	0.3583 and 0.6363
largest diff. peak and hole	7.67 and −4.85 e.Å^{-3}

[a] $R = \sum||F_o| - |F_c||/\sum|F_o|$, $wR = \sum[w(|F_o|^2 - |F_c|^2)^2]/\sum[w(|F_o|^4)]]^{1/2}$ and $w = 1/(\sigma^2(I) + 0.0016I^2)$.

Various corrections were made to the data, such as subtraction of background and container, Compton, and fluorescence scattering, geometric corrections, absorption, and so forth.[74] Corrections were made using the program PDFgetX2.[75] Finally, $S(Q)$ was truncated at Q_{max} of 27 Å^{-1} before the PDF was calculated. Simulations were carried out using PDFfit2.[76]

RESULTS AND DISCUSSION

Synthesis and Structure. All reported compounds (**1**−**3**) were synthesized using a thiophosphate flux at 900 °C, employing excess chalcogenide flux to stabilize the Sn(II) oxidation state. The $ASnPS_4$ compounds have a two-dimensional layered structure formed by corrugated layers of $[SnPS_4]_n^{n-}$ separated by alkali metal cations. Compounds **1** and **2** are isostructural whereas the Cs analogue (**3**) has a commensurately modulated superstructure with a modulation vector q = 1/4a* + 1/4c*. As **1** and **2** are isostructural, this discussion will focus on the structure of **1**. Compound **1** crystallizes as yellow-orange polyhedral crystals in the monoclinic space group $P2_1/c$. A representative view of the layered structure of **1** is shown in Figure 1A and 1B, viewing along the [010] direction, which clearly depicts the alternating $[SnPS_4]_n^{n-}$ layers extending throughout the unit cell. The crystallographic summary, selected bond distances and bond angles for **1**, are listed in Tables 1−4. The corrugated layers are composed of SnS_3 pyramids and PS_4 tetrahedral units. The divalent tin atoms are three coordinate with pyramidal geometry; consequently, the lone pair on tin appears to be stereochemically active. The SnS_3 pyramids and the PS_4 tetrahedral units share corners and involves three Sn−S bonds and three P−S bonds, resulting in one bond of the PS_4 unit always remaining terminal. The alternating up and down fashion of the building units gives rise to a layer along the [010] direction (Figure 2A). This causes the directions of the SnS_3 pyramids to be antiparallel to one another, leading to a centrosymmetric structure.

The $[SnPS_4]_n^{n-}$ layers contain two different types of rings: 16-member, crown-shaped rings and 8-member, chair-shaped rings, in which the metal ion alternates between Sn and P when following the perimeter of each type of ring (Figure 2B). The larger 16-member ring is formed by corner-sharing of two of the Sn−S bonds in the SnS_3 pyramid with two PS_4 units. Interestingly, the terminal P−S bond from each PS_4 unit is oriented in an alternating up and down fashion facing inside the 16-member ring. In this way, each SnS_3 pyramid is connected to three PS_4 tetrahedra through corner sharing. The closest distance between two adjacent layers is ∼1.90 Å, which suggests efficient packing and explains the relatively low anisotropic displacement parameters of K atoms in the structure as the spacing between layers is only slightly larger than the ionic radius of the potassium ion, Figure 3B. The potassium cations sit between the layers surrounded by the sulfur atoms in a distorted bicapped trigonal prismatic environment with an average K−S bond distance of 3.35 Å.

In compound **1**, the Sn(II) centers are coordinated to three S atoms in a pyramidal geometry with the $5s^2$ electron lone-pair pointing toward the apex of the pyramid along the [010] direction. The three Sn−S distances vary from 2.7158(4) Å [Sn(1)−S(2)] to 2.8017 Å [Sn(1)−S(1)] and 2.8092(6) Å [Sn(1)−S(4)] (Figure 3A). There are also long, weak Sn−S intralayer interactions with adjacent PS_4 groups at distances ranging from 3.0306(10) to 3.9574(14) Å. The S−Sn−S angles range from 78.365(2)° to 87.490(3)°, possibly distorted from repulsion between the $5s^2$ lone pair electrons and the Sn−S bonding electrons. This type of Sn(II) coordination environment is extremely rare in chalcogenides, although some examples exist in organometallic chemistry.[77−79] In the tetrahedral $[PS_4]^{3-}$ unit, there are two types of P−S bonds: three bridging and one terminal. The bridging P−S bond lengths are 2.060(3) Å [P(1)−S(1)], 2.048(3) Å [P(1)−S(2)], and 2.029(5) Å [P(1)−S(4)] whereas the terminal bond [P(1)−S(3)] is slightly shorter at 2.013(3) Å.

The average P−S bond distance in the PS_4 tetrahedra is 2.038 Å, which is in good agreement with the sum of the ionic radii (not assuming a purely ionic P−S bond) found in other ortho-thiophosphates such as $KNiPS_4$,[80,81] $KPdPS_4$,[82] $KEuPS_4$,[43] $KPbPS_4$,[51] $TlSnPS_4$,[83] and $TlPbPS_4$.[84] The S−P−S angles are indicative of regular tetrahedra with a slight deviation from the ideal tetrahedral geometry in which the average S−P−S angle should be 109.4°. The S−P−S angles range from 108.10(2)° to 110.26(5)°, showing only a slight deviation from the ideal value. The K−S distances range from 3.238(7) to 3.512(7) Å, among which the K−S(2) distance is the longest.

dx.doi.org/10.1021/ic301456m | Inorg. Chem. 2012, 51, 11562−11573

Table 7. Atomic Coordinates ($\times 10^4$), Fourier Components of the Displacive Modulation ($\times 10^4$), Occupancy, and Equivalent Isotropic Displacement Parameters ($Å^2 \times 10^4$) for $CsSnPS_4$ at 100.0(3) K with Estimated Standard Deviations in Parentheses

atom	wave	x	y	z	occupancy	U_{eq}[a]
Cs(1)	0	4235(2)	2500	2991(1)	1	16(1)
	sin,1	0	103(2)	0		
	cos,1	0	−371(2)	0		
	sin,2	−89(2)	0	−1(1)		
	cos,2	0	0	0		
Cs(2)	0	9210(2)	7500	2007(1)	1	18(1)
	sin,1	0	81(2)	0		
	cos,1	0	−384(2)	0		
	sin,2	257(3)	0	−50(2)		
	cos,2	0	0	0		
Sn(1)	0	7071(2)	2500	201(1)	1	11(1)
	sin,1	0	875(2)	0		
	cos,1	0	−368(2)	0		
	sin,2	−4(2)	0	−10(1)		
	cos,2	0	0	0		
Sn(2)	0	2080(2)	7500	4794(1)	1	12(1)
	sin,1	0	752(2)	0		
	cos,1	0	−316(2)	0		
	sin,2	−24(2)	0	4(1)		
	cos,2	0	0	0		
P(1)	0	7235(6)	7500	4016(2)	1	13(1)
	sin,1	0	−422(7)	0		
	cos,1	0	−326(6)	0		
	sin,2	130(10)	0	−39(4)		
	cos,2	0	0	0		
P(2)	0	7770(5)	7500	9015(2)	1	10(1)
	sin,1	0	−324(7)	0		
	cos,1	0	195(5)	0		
	sin,2	57(4)	0	5(2)		
	cos,2	0	0	0		
S(1)	0	6701(5)	7500	5143(2)	1	14(1)
	sin,1	0	−808(6)	0		
	cos,1	0	−318(5)	0		
	sin,2	265(8)	0	−12(3)		
	cos,2	0	0	0		
S(2)	0	8929(4)	9939(3)	3773(2)	1	16(1)
	sin,1	20(5)	−409(5)	84(2)		
	cos,1	−46(5)	−218(4)	−21(2)		
	sin,2	59(3)	13(4)	−27(2)		
	cos,2	0	0	0		
S(3)	0	8319(5)	7500	146(2)	1	12(1)
	sin,1	0	−655(6)	0		
	cos,1	0	333(5)	0		
	sin,2	259(9)	0	2(3)		
	cos,2	0	0	0		
S(4)	0	4352(6)	7500	3486(2)	1	14(1)
	sin,1	0	100(6)	0		
	cos,1	0	−374(7)	0		
	sin,2	−42(6)	0	6(3)		
	cos,2	0	0	0		
S(5)	0	651(6)	7500	8484(2)	1	11(1)
	sin,1	0	110(5)	0		
	cos,1	0	357(6)	0		
	sin,2	144(12)	0	21(5)		
	cos,2	0	0	0		
S(6)	0	6074(3)	9936(3)	8774(2)	1	13(1)
	sin,1	8(4)	−281(4)	81(2)		
	cos,1	−88(4)	80(3)	51(2)		
	sin,2	43(2)	−11(2)	8(2)		
	cos,2	0	0	0		

dx.doi.org/10.1021/ic301456m | Inorg. Chem. 2012, 51, 11562−11573

Table 7. continued

[a] U_{eq} is defined as one-third of the trace of the orthogonalized U_{ij} tensor.

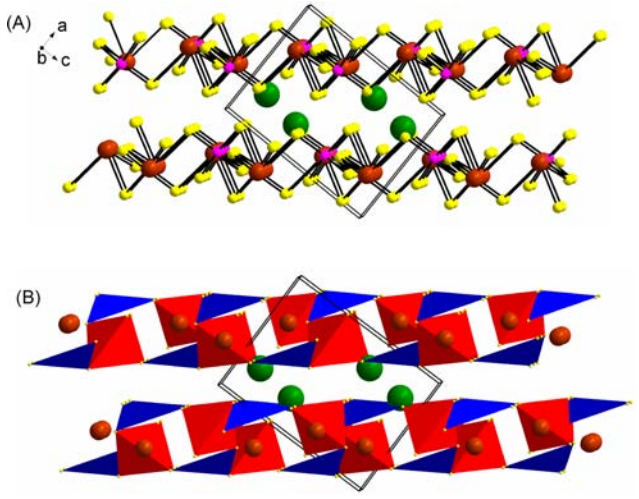

Figure 1. (A) Layered structure of **1** showing corrugated $[SnPS_4]_n^{n-}$ layers within the unit cell. Color codes of atoms in ball and stick representation: K in green, Sn in red, P in pink, and S in yellow. (B) Polyhedral representation of the layered structure of **1**; SnS_3 pyramid: blue polyhedra, PS_4 tetrahedra: red polyhedra.

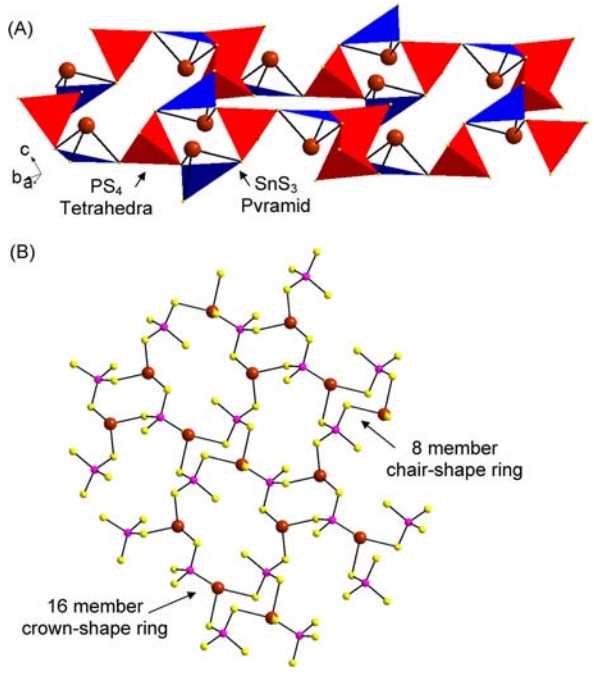

Figure 2. (A) Polyhedral representation of $[SnPS_4]_n^{n-}$ layer in **1** showing corner sharing SnS_3 and PS_4 polyhedra; SnS_3 pyramids are arranged in an alternating up and down fashion within the layer. (B) Large 16 member rings and small 8 member rings formed within $[SnPS_4]_n^{n-}$ layer through corner sharing of SnS_3 pyramids and PS_4 tetrahedra.

The potassium atom forms a KS_8 polyhedron that shares edges with three neighboring PS_4 tetrahedra (Figure 3C).

CsSnPS$_4$: A Modulated Structure. Compound **3** crystallizes in the monoclinic superspace group $P2_1(\alpha\beta0)0$ with a commensurate q-vector at 1/4a* + 1/4c*, Table 6. The structure of **3** is similar to that of **1** and **2** in which layers of

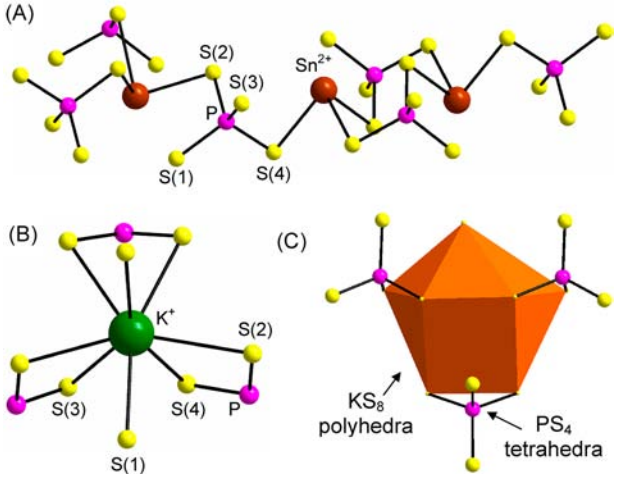

Figure 3. (A) Coordination environment of three coordinate Sn^{2+} in **1**. (B) Eight coordinate K^+ ion forming KS_8 polyhedra. (C) Edge sharing between KS_8 polyhedra and PS_4 tetrahedra.

$[SnPS_4]_n^{n-}$ alternate with Cs atoms, Figure 4. The layers are composed of SnS_3 pyramids and PS_4 tetrahedral units. Because

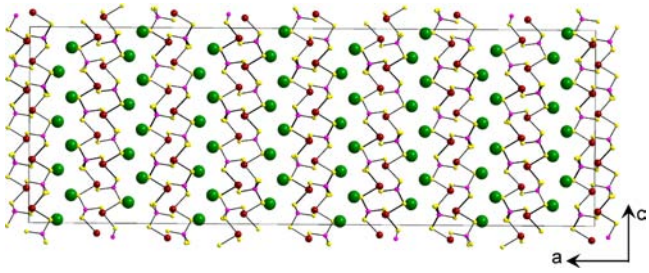

Figure 4. Modulated structure of the commensurate superstructure of compound **3** (4a × 4c supercell) viewed along [001] direction. The alternating $[SnPS_4^-]$ layers have different phosphorus coordination environments, thus resulting in two crystallographically different types of phosphorus atoms in the structure. Color codes of atoms in ball and stick representation: Cs in green, Sn in red, P in pink, and S in yellow.

of the superstructure the position of mainly Sn atoms fluctuate around the average position with a distorted pyramidal geometry. The bond length distribution between Sn and S atoms varies from a minimum of 2.615(8) Å to a maximum of 3.585(7) Å. The S−Sn−S bond angles range from 58.5(3)° to 83.8(5)Å. The PS_4 units rotate and distort to accommodate the changes in the SnS_3 units. The minimum P−S distance is 1.962(8) Å and the maximum is 2.117(8) Å while the angle distribution is 103.4(3)° to 115.5(4)°. The Cs−S distances range from 3.399(8) Å to 3.815(7) Å. A complete list of bond distances and angles can be found in Tables 8 and 9 (a list of grouped bond angle distributions is reported in the Supporting Information).

The $[SnPS_4]_n^{n-}$ layers in compound **3** have a different connectivity compared to that of **1**. In compound **1**, the layers contain two types of rings whereas the $[SnPS_4]_n^{n-}$ layers in **3** contain three different types of rings: 16, 12, and 8 member rings (Figure 5A). In compound **3**, the sides of each 16-member ring are surrounded by two 8-member rings and six

dx.doi.org/10.1021/ic301456m | Inorg. Chem. 2012, 51, 11562−11573

Table 8. Anisotropic Displacement Parameters ($Å^2 \times 10^3$) for $CsSnPS_4$ at 100.0(3) K with Estimated Standard Deviations in Parentheses[a]

label	U_{11}	U_{22}	U_{33}	U_{12}	U_{13}	U_{23}
Cs(1)	23(1)	17(1)	7(1)	0	−2(1)	0
Cs(2)	27(1)	15(1)	13(1)	0	2(1)	0
Sn(1)	11(1)	9(1)	14(1)	0	1(1)	0
Sn(2)	11(1)	13(1)	12(1)	0	0(1)	0
P(1)	15(2)	11(2)	14(2)	0	2(2)	0
P(2)	7(2)	19(2)	3(2)	0	2(2)	0
S(1)	16(2)	11(2)	14(2)	0	1(1)	0
S(2)	15(2)	15(1)	17(2)	−3(1)	1(1)	0(1)
S(3)	16(2)	14(2)	7(2)	0	1(1)	0
S(4)	12(2)	19(2)	12(2)	0	−1(2)	0
S(5)	10(2)	17(2)	7(2)	0	2(2)	0
S(6)	11(2)	12(1)	15(2)	1(1)	−1(1)	−2(1)

[a]The anisotropic displacement factor exponent takes the form: $-2\pi^2[h^2a^{*2}U_{11} + ... + 2hka^*b^*U_{12}]$.

Table 9. Grouped Bond Lengths Distributions [Å] for $CsSnPS_4$ at 100.0(3) K with Estimated Standard Deviations in Parentheses

atom	average distance	minimum distance	maximum distance
Cs(1)−S(1)	3.463(4)	3.415(4)	3.511(4)
Cs(2)−S(3)	3.447(3)	3.444(3)	3.450(3)
Sn(1)−P(2) × 2	4.074(4)	3.497(4)	4.673(4)
Sn(1)−P(2)	3.380(5)	3.366(5)	3.395(5)
Sn(1)−S(3) × 2	3.515(4)	2.709(4)	4.326(4)
Sn(1)−S(3)	3.497(5)	3.411(5)	3.584(5)
Sn(1)−S(3)	2.987(5)	2.970(5)	3.004(5)
Sn(1)−S(5)	2.778(4)	2.775(4)	2.781(4)
Sn(1)−S(6) × 2	3.226(6)	2.945(6)	3.562(5)
Sn(1)−S(6) × 2	3.200(5)	2.776(6)	3.606(5)
Sn(2)−P(1)	3.380(5)	3.350(5)	3.410(5)
Sn(2)−S(1)	3.491(5)	3.368(5)	3.613(6)
Sn(2)−S(1)	2.993(5)	2.976(5)	3.010(5)
Sn(2)−S(1) × 2	3.512(4)	2.705(4)	4.328(4)
Sn(2)−S(2) × 2	3.202(5)	2.768(6)	3.622(6)
Sn(2)−S(2) × 2	3.237(5)	2.942(5)	3.619(5)
Sn(2)−S(4)	2.765(5)	2.757(5)	2.772(5)
P(1)−S(1)	2.068(5)	2.067(5)	2.068(5)
P(1)−S(2) × 2	2.024(6)	2.004(7)	2.038(7)
P(1)−S(4)	2.035(6)	2.032(6)	2.038(6)
P(2)−S(3)	2.079(5)	2.070(5)	2.088(5)
P(2)−S(5)	2.034(6)	2.034(6)	2.034(6)
P(2)−S(6) × 2	2.023(6)	2.007(6)	2.034(6)
S(1)−S(2) × 2	3.297(6)	3.256(6)	3.341(7)
S(1)−S(4)	3.343(6)	3.331(6)	3.356(6)
S(2)−S(2)	3.345(7)	3.338(7)	3.351(7)
S(2)−S(2)	3.512(7)	3.492(7)	3.532(7)
S(2)−S(4)	3.338(7)	3.293(7)	3.375(7)
S(3)−S(5)	3.348(5)	3.336(5)	3.360(5)
S(3)−S(6) × 2	3.305(6)	3.263(6)	3.355(6)
S(5)−S(6) × 2	3.339(7)	3.295(7)	3.380(7)
S(6)−S(6)	3.343(7)	3.336(7)	3.350(7)

12-member rings. In the case of **1**, each of the 16-member rings is surrounded by four 8-member rings and another four 16-member rings. The packing of the alkali metal ions is similar in both **1** and **3** and are between the layers in a zigzag fashion (Figure 5B). The reason behind puckering of the $[SnPS_4]_n^{n-}$ layers in all these compounds can be explained based on the electronic repulsion between the lone pair electrons present on Sn(II) ions. Figure 6 shows a comparison between the distorted $[SnPS_4]_n^{n-}$ layer in **3** and an ideal situation where the layers would have no distortion. In the distorted configuration the row of Sn(II) atoms are arranged in a zigzag fashion, hence canceling the electronic repulsion between the lone pair of electrons on each Sn(II). Upon removing the distortion the $[SnPS_4]_n^{n-}$ layers assume a configuration where only 12-member rings are present and all the Sn(II) atoms are arranged in a linear fashion, resulting in all the lone pairs pointing in the same direction. This results in a higher energy configuration of the $[SnPS_4]_n^{n-}$ layers, which is thermodynamically unfavorable. Hence all the $ASnPS_4$ compounds crystallize in a structure in which the $[SnPS_4]_n^{n-}$ layers are puckered. The extent of puckering of the $[SnPS_4]_n^{n-}$ layers increases in going from compound **1** to **3**, which is believed to arise from the increase in the size of alkali metal ions. The $[SnPS_4]_n^{n-}$ layers assume an extra 12-membered ring in **3** to accommodate the much larger Cs^+ ions, resulting in a modulated superstructure for $CsSnPS_4$.

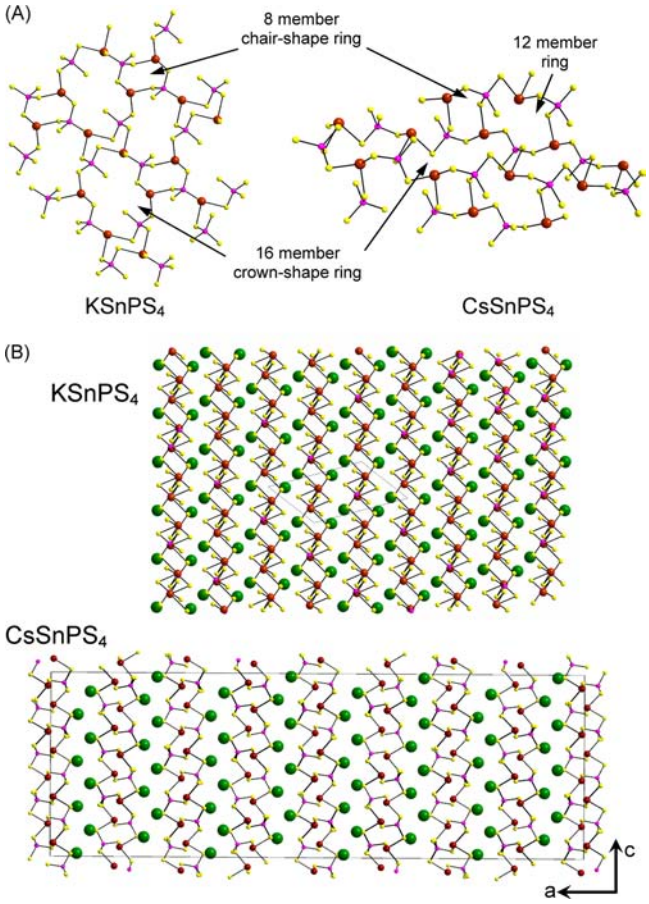

Figure 5. (**A**) Comparison between the $[SnPS_4]_n^{n-}$ layers of $KSnPS_4$ (**1**) and $CsSnPS_4$ (**3**) compounds. (**B**) Comparison between packing of alkali metal ions and $[SnPS_4]_n^{n-}$ layers within an extended 4a × 4c cell of **1** and 4a × 4c super cell of **3**. Color codes of atoms in ball and stick representation: K and Cs in green, Sn in red, P in pink, and S in yellow.

The only other known tin ortho-thiophosphate with a similar formula is $TlSnPS_4$,[83] which crystallizes in the orthorhombic $Pna2_1$ space group and is isostructural with $TlPbPS_4$[84] and $TlEuPS_4$.[27] The structure of $TlSnPS_4$ consists of puckered layers of condensed chains of adjacent face-sharing $[TlS_6]$ and

dx.doi.org/10.1021/ic301456m | Inorg. Chem. 2012, 51, 11562−11573

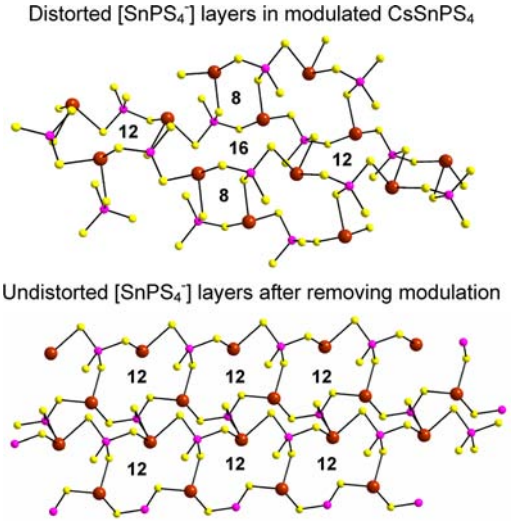

Figure 6. Comparison between $[SnPS_4]_n^{n-}$ layers in modulated structure of **3** with the undistorted $[SnPS_4]_n^{n-}$ layer obtained upon removing modulation. The numbers inside the rings indicate the number of members of each ring.

$[SnS_6]$ prisms, which are then joined by $[PS_4]$ tetrahedra. The tin atom has a more common octahedral coordination in $TlSnPS_4$. Another well-known Sn(II) thiophosphate is $Sn_2P_2S_6$, which is well-known for its ferroelectric, piezoelectric properties, and so forth.[85]

Physical Characterization. The solid state electronic absorption spectra of the crystalline compounds **1**, **2**, and **3** (Figure 7) showed very strong absorption edges at ~2.0−2.2

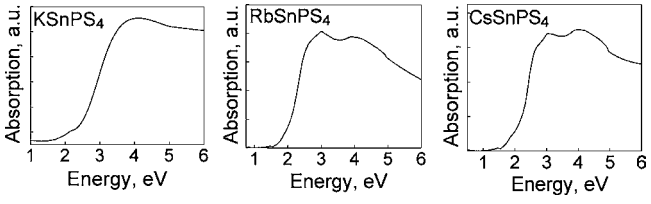

Figure 7. Solid state optical absorption spectra for crystalline **1**−**3**.

eV. The optical absorption spectra are believed to originate from charge transfer from the S-based valence bands to Sn-based conduction bands.[49] Raman spectra for the crystalline compounds **1**, **2**, and **3** are very active and show characteristic peaks for the tetrahedral $[PS_4]^{3-}$ unit and metal−sulfur bonds. The spectra for the crystalline potassium (**1**) and rubidium (**2**) salts are similar to each other and have peaks at ~158(m), 218(m), 267(m), 317(w), 417(s), 527(m), 549(m), and 572(m) cm^{-1} (Figure 8A). The strong peaks at ~420 cm^{-1} are due to the A_1 symmetric stretch of PS_4 whereas the peaks at ~570 cm^{-1} arise from the P−S asymmetric stretching vibrations of the tetrahedral $[PS_4]^{3-}$ unit. The characteristic peak for bending vibrations of P−S bonds in the PS_4 unit appear at 314 cm^{-1}.[43] The peaks at ~150−160 cm^{-1} are due to Sn−S stretching vibrations.

The Raman spectrum for the crystalline cesium salt (compound **3**) shows all characteristic peaks as described for the two other salts as well as an additional peak at 347 cm^{-1} arising from the bending vibrations of P−S bonds. This peak is also observed in the spectra for **1** and **2** but with much weaker intensity. It is much more prominent in the case of the cesium

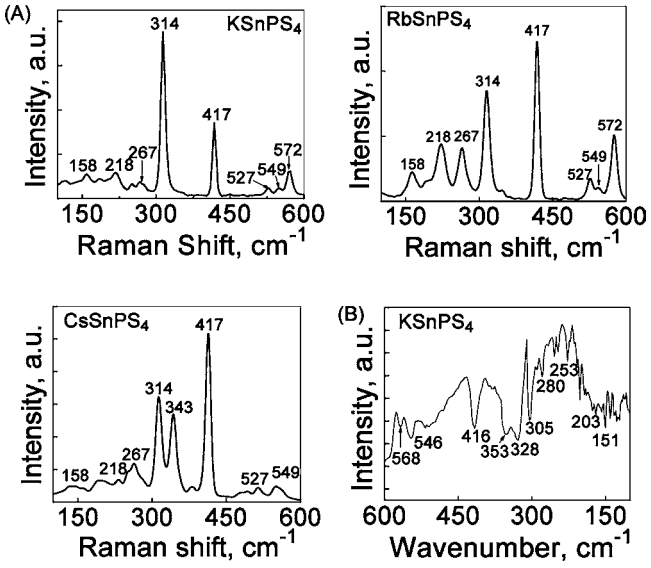

Figure 8. (**A**) Raman spectra for crystalline **1**, **2**, and **3**. (**B**) Far-IR spectra for crystalline $KSnPS_4$.

salt possibly because of the superstructuring. The far-IR spectra for the thiophosphates (compounds **1**−**3**) also showed metal−sulfur and P−S stretching modes as well as characteristic S−P−S bending vibration modes (Figure 8B). The peaks between 400 and 500 cm^{-1} are characteristic of stretching vibration modes of P−S bonds whereas those around 300−350 cm^{-1} are due to S−P−S bending modes. Metal−sulfur stretching vibrations give rise to the peak at 150 cm^{-1}.

Differential thermal analysis (DTA) was used to characterize compounds **1**, **2**, and **3**. These layered materials were not ground for use in DTA experiments because they tend to smear into agglomerates. All three compounds were heated at a rate of 10 °C/min to 600 °C and cooled at 10 °C/min to 150 °C, for two consecutive cycles in the DTA. All three compounds exhibit reproducible melting and recrystallization temperatures during the first and second heating and cooling cycles, indicating that they melt and recrystallize congruently. Representative plots for the first cycle of the DTA obtained for **1**, **2**, and **3** are shown in Figure 9A. The second cycles of the DTA for all three compounds are shown in the Supporting Information, which have similar melting and crystallization points. $KSnPS_4$ (**1**) exhibits a melting endotherm at 530 °C and a recrystallization exotherm at 502 °C, $RbSnPS_4$ (**2**) melts at 560 °C and recrystallizes at 530 °C, and $CsSnPS_4$ (**3**) melts at 536 °C and recrystallizes at 518 °C. The X-ray powder diffraction pattern of the DTA residue from $ASnPS_4$ is identical to that from the corresponding starting materials (Figure 9B).

Solid state ^{31}P NMR spectra were recorded for compounds **1** and **3** as the crystallographic environment of the PS_4 group is different in these two compounds (Figure 10). In the case of **1**, the ^{31}P NMR spectrum shows a strong single peak at a chemical shift of 80 ppm as expected for the one crystallographically unique PS_4 group present in the compound. Compound **3** has two crystallographically different types of PS_4 groups in the structure (Figure 4), which clearly explains the appearance of two peaks in the solid state NMR spectrum. The main peaks for compound **3** appear at 94.7 and 97.8 ppm with their spinning sidebands clearly marked. Similar solid state NMR shifts were observed for the modulated structures $K_{1.5}Bi_{2.5}(PS_4)_3$ and $K_9Bi(PS_4)_4$.[86]

dx.doi.org/10.1021/ic301456m | Inorg. Chem. 2012, 51, 11562−11573

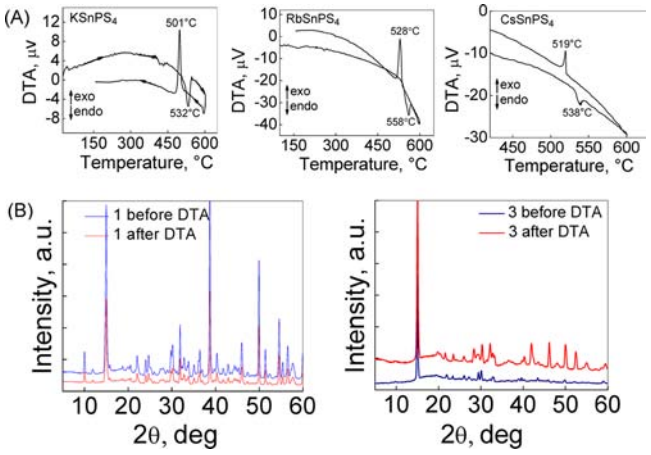

Figure 9. (**A**) Differential thermal analysis (DTA) plots of compounds **1**, **2**, and **3** showing congruent melting of the crystalline compounds in the first cycle of DTA. (See the Supporting Information for the second DTA cycle) (**B**) X-ray powder diffraction patterns for compounds **1** and **3** before and after the DTA experiments showing the recovery of the crystalline compounds after DTA.

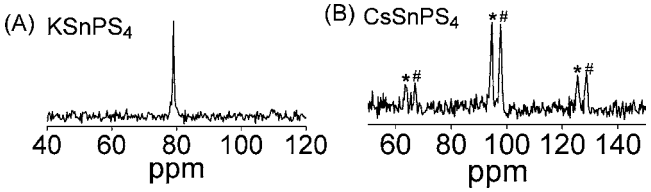

Figure 10. Solid state ^{31}P NMR spectra for (**A**) $KSnPS_4$ and (**B**) $CsSnPS_4$ (Spinning side-bands are grouped under alike symbols).

Glassy thiophosphate materials such as $Li_4P_2S_7$, $LiPS_4$, and $AgPS_3$[87,88] are of interest as good ionic conductors[89,90] as their conductivity is several orders of magnitude higher than their oxide analogues. The higher polarizability of the sulfur atom contributes to the higher Li^+ ion mobility.[91] Thiophosphate glasses are also good thermoplastic materials and are used as lubricants in mechanical applications[92,93] for which the thermal expansion coefficient can be tuned by varying the P_xS_y content. Ternary and quaternary thiophosphate glass systems have been widely studied such as binary $Li_2S-P_2S_5$,[94,95] Li_2S-SiS_2 and quaternary $Li_2S-P_2S_5-SiS_2-LiI$ glass systems,[96] the related SiS_2 based glasses for solid state battery applications[97] and so forth. As the $ASnPS_4$ compounds were found to be congruently melting, we investigated the properties of glassy $ASnPS_4$ materials.

Compounds **1**, **2**, and **3** formed glasses upon melt quenching. The glassy compounds were characterized with X-ray diffraction, Raman spectroscopy, and electronic absorption spectroscopy. A representative SEM image of glassy **1** is shown in Figure 11A and EDS shows the quaternary elemental composition of the glass. The band gap measurement of glassy **1** showed a well-defined band gap at 2.07 eV, indicating that it is a semiconducting glassy material (Figure 11B). As is typically observed, the band gap of the glassy form of **1** was found to be lower than that of crystalline **1**, most likely because of formation of lattice defects in the glass.[98,99] The X-ray powder pattern of glassy **1** (Figure 11C) shows broad peaks consistent with loss of long-range order in the material. The Raman spectrum of glassy **1** shows three peaks at 314(s), 417(s), and 572(w) cm^{-1}, which are characteristic for P−S bond bending, symmetric, and asymmetric stretching vibrations, respectively (Figure 11D). The Raman peaks for glassy **1** are broader than

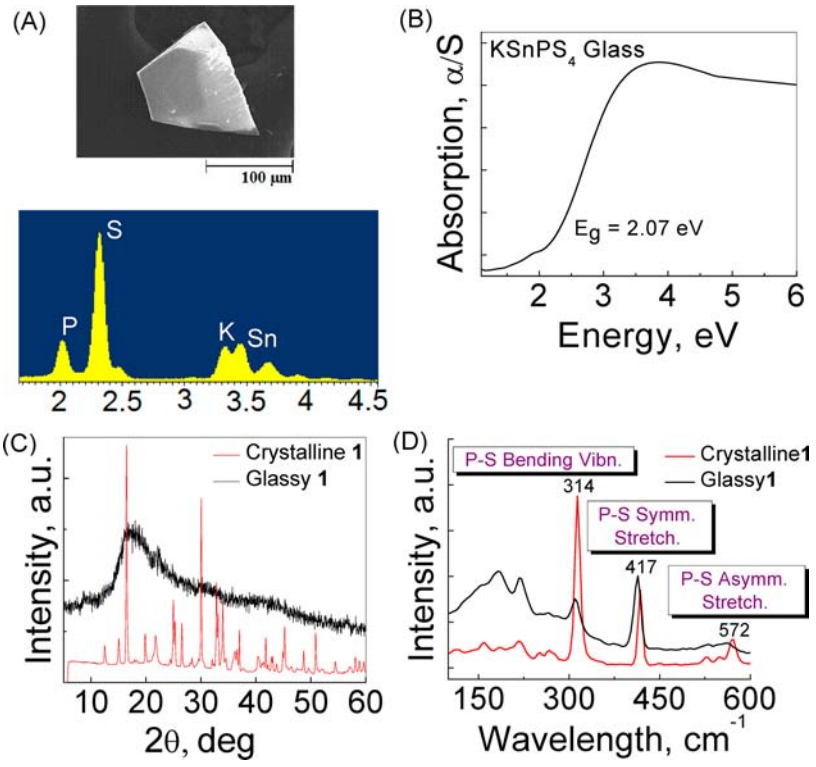

Figure 11. (**A**) SEM image of glassy **1** and EDS plot showing the quaternary composition. (**B**) Solid state electronic absorption of glassy **1** showing a band gap of 2.07 eV. (**C**) Comparison between X-ray powder diffraction patterns of crystalline and glassy **1**. (**D**) Comparison between Raman spectra of crystalline and glassy **1**, showing characteristic peaks from the $[PS_4]^{3-}$ units present in the glassy form.

dx.doi.org/10.1021/ic301456m | *Inorg. Chem.* 2012, 51, 11562−11573

those for crystalline **1** because of a lowering in symmetry of the structure in the glassy phase. Also the similarity in the Raman spectra of both glassy and crystalline **1** clearly shows that the short-range ordering of atoms is preserved in the glassy phase to some extent.

The atomic structure of glassy $KSnPS_4$ was further studied and compared against its crystalline phase using the pair distribution function (PDF) method. This method has been successfully used for the structural characterization of liquids and glasses.[100] The PDF plot of glassy $KSnPS_4$ is shown in Figure 12. Atomic pair correlations expressed as distinct peaks

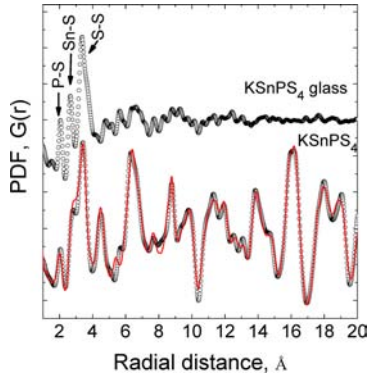

Figure 12. Pair Distribution Function (PDF) analysis plot for crystalline **1** and glassy **1**. Red line represents the fit of the crystallographic model.

are observed up to ~4 Å. More specifically, the peak around 2 Å arises from the P−S bonds, the one around 2.7 Å corresponds to Sn−S, and the broad peak around 3.4 Å can be assigned to K−S, Sn- - -Sn, and S−S atomic pairs. Similar interatomic vectors were observed in the crystalline phase of $KSnPS_4$, Figure 12. Furthermore, the refinement of the crystallographically obtained model against the experimental data (red line in Figure 12) yielded an excellent agreement factor (~16%) by refining only cell parameters and thermal factors, verifying the correctness of the structure refinement.

DTA of the crystalline compounds showed that the crystal to glass transition is very facile and can be repeatedly performed. A good phase change material should also have a facile glass to crystal transition. To check how well the glass can be crystallized upon heating, a DTA experiment was performed on glassy **1**. A reaction mixture was prepared to synthesize **1** using a direct combination ratio of the starting materials, K_2S/Sn/P/S, and heated inside a furnace at 900 °C for a few hours. The red hot melt in the sealed fused silica tube was plunged into cold water to get a crimson red colored glass. A similar experiment was done using the flame-melting/rapid quenching method starting from the starting reagents and pure crystalline **1**. The glassy phase of **1** was then put inside a DTA tube, sealed under vacuum, heated at 10 °C/min to 600 °C and cooled to 50 °C; this was repeated twice. The DTA plot in Figure 13 shows that glassy **1** melts at 531 °C and recrystallizes at 504 °C over repeated cycles of DTA. The melting and recrystallization points of glassy **1** match almost exactly with that of crystalline **1**. This confirms that **1** is a phase-change material.[99,101−105]

Generally, the glassy forms of phase-change materials crystallize upon heating well before melting. The fact that the glassy form of **1** first melts upon heating instead of crystallizing is unusual and indicates the glass form is fully kinetically stabilized. To verify that there is indeed no crystallization

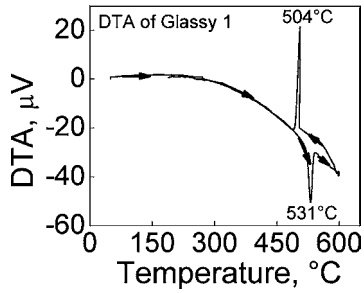

Figure 13. Differential thermal analysis (DTA) plot of glassy **1**.

before melting we carried out a DTA experiment where glassy **1** was heated at a slower rate (5 °C/min) up to 400 °C and cooled back down. This cycle was repeated twice and no exothermic crystallization event that can be attributed to a crystallization point was observed (Figure 14A). Also, the X-ray powder diffraction pattern recorded before and after DTA indicated the same glassy phase of compound **1** (Figure 14B).

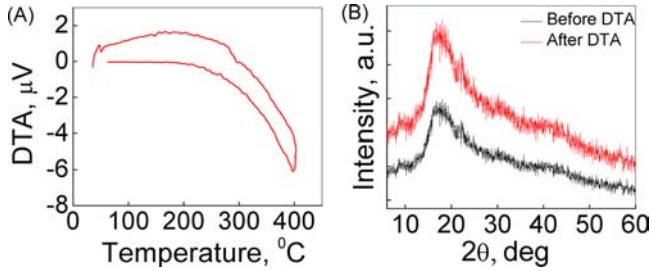

Figure 14. (A) DTA plot of glassy **1** up to 400 °C; (B) X-ray powder diffraction pattern recorded before and after DTA.

CONCLUDING REMARKS

A new family of quaternary tin(II) thiophosphate compounds was synthesized using the molten flux technique. These compounds have an unusual divalent tin metal center surrounded by $[PS_4]^{3-}$ units forming SnS_3 pyramids arranged in a two-dimensional layered structure. The alkali metal cations are situated between the layers and are localized. All three compounds appear to melt congruently and powder X-ray diffraction shows recovery of the crystalline materials after crystallization of the melts. The thiophosphate compounds are good glass forming materials that do not crystallize upon heating. The local structure of the glassy phases is similar to that of the corresponding crystalline phases as indicated by Raman spectroscopy and X-ray pair distribution function analysis.

ASSOCIATED CONTENT

Supporting Information

Details for the physical and analytical techniques used in the present work, experimental versus calculated powder X-ray diffraction patterns of 1, and CIF files for **1** and **3**. This material is available free of charge via the Internet at http://pubs.acs.org.

AUTHOR INFORMATION

Corresponding Author

*E-mail: m-kanatzidis@northwestern.edu.

Notes

The authors declare no competing financial interest.

■ ACKNOWLEDGMENTS

Financial support from the NSF (DMR-1104965) is gratefully acknowledged. Use of the Advanced Photon Source and BESSRC facility (11-ID-B) was supported by the U.S. Department of Energy, Office of Science, and Office of Basic Energy Sciences, under Contract W-31-109-Eng-38.

■ REFERENCES

(1) Carpenti, Cd; Nitsche, R. *Mater. Res. Bull.* **1974**, *9*, 1097−1100.
(2) Flerova, S. A.; Bochkov, O. E.; Kudzin, A. Y.; Krochmal, Y. D. *Ferroelectrics* **1982**, *45*, 131−134.
(3) Barsamian, T. K.; Khasanov, S. S.; Shekhtman, V. S.; Vysochanskii, Y. M.; Slivka, V. Y. *Ferroelectrics* **1986**, *67*, 47−54.
(4) Rogach, Y. D.; Savchenko, E. A.; Sandjiev, D. N.; Protsenko, N. P.; Rodin, A. I. *Ferroelectrics* **1988**, *83*, 179−185.
(5) Grigas, J.; Kalesinskas, V.; Lapinskas, S.; Gurzan, M. I. *Phase Transitions* **1988**, *12*, 263−274.
(6) Valevichius, V.; Samulionis, V.; Skritskij, V. *Ferroelectrics* **1988**, *79*, 519−522.
(7) Grigas, J.; Kalesinskas, V.; Lapinskas, S. *Ferroelectrics* **1988**, *80*, 873−876.
(8) Rogach, E. D.; Sviridov, E. V.; Arnautova, E. A.; Savchenko, E. A.; Protsenko, N. P. *Zh Tekh Fiz+* **1991**, *61*, 201−204.
(9) Bourdon, X.; Maisonneuve, V.; Cajipe, V. B.; Payen, C.; Fischer, J. E. *J. Alloys Compd.* **1999**, *283*, 122−127.
(10) Galdamez, A.; Manriquez, V.; Kasaneva, J.; Avila, R. E. *Mater. Res. Bull.* **2003**, *38*, 1063−1072.
(11) Kroupa, J.; Tyagur, Y. I.; Grabar, A. A.; Vysochanskii, Y. M. *Ferroelectrics* **1999**, *223*, 421−428.
(12) Misuryaev, T. V.; Murzina, T. V.; Aktsipetrov, O. A.; Sherstyuk, N. E.; Cajipe, V. B.; Bourdon, X. *Solid State Commun.* **2000**, *115*, 605−608.
(13) Liao, J. H.; Marking, G. M.; Hsu, K. F.; Matsushita, Y.; Ewbank, M. D.; Borwick, R.; Cunningham, P.; Rosker, M. J.; Kanatzidis, M. G. *J. Am. Chem. Soc.* **2003**, *125*, 9484−9493.
(14) Chung, I.; Malliakas, C. D.; Jang, J. I.; Canlas, C. G.; Weliky, D. P.; Kanatzidis, M. G. *J. Am. Chem. Soc.* **2007**, *129*, 14996−15006.
(15) Banerjee, S.; Malliakas, C. D.; Jang, J. I.; Ketterson, J. B.; Kanatzidis, M. G. *J. Am. Chem. Soc.* **2008**, *130*, 12270−12272.
(16) Kanatzidis, M. G. *Curr. Opin. Solid State Mater. Sci.* **1997**, *2*, 139−149.
(17) Chondroudis, K.; Kanatzidis, M. G. *J. Solid State Chem.* **1998**, *136*, 79−86.
(18) Mccarthy, T. J.; Kanatzidis, M. G. *J. Chem. Soc., Chem. Commun.* **1994**, 1089−1090.
(19) Wu, Y.; Bensch, W. *CrystEngComm* **2010**, *12*, 1003−1015.
(20) Dorhout, P. K.; Malo, T. M. *Z. Anorg. Allg. Chem.* **1996**, *622*, 385−391.
(21) Tremel, W.; Kleinke, H.; Derstroff, V.; Reisner, C. *J. Alloys Compd.* **1995**, *219*, 73−82.
(22) Chondroudis, K.; Kanatzidis, M. G. *J. Solid State Chem.* **1998**, *138*, 321−328.
(23) Chondroudis, K.; Kanatzidis, M. G. *Angew. Chem., Int. Ed. Engl.* **1997**, *36*, 1324−1326.
(24) Derstroff, V.; Tremel, W. *Chem. Commun.* **1998**, 913−914.
(25) Gieck, C.; Derstroff, V.; Block, T.; Felser, C.; Regelsky, G.; Jepsen, O.; Ksenofontov, V.; Gutlich, P.; Eckert, H.; Tremel, W. *Chem.—Eur. J.* **2004**, *10*, 382−391.
(26) Chondroudis, K.; McCarthy, T. J.; Kanatzidis, M. G. *Inorg. Chem.* **1996**, *35*, 840−844.
(27) Carrillo-Cabrera, W.; Peters, K.; von Schnering, H. G.; Menzel, F.; Brockner, W. *Z. Anorg. Allg. Chem.* **1995**, *621*, 557−561.
(28) Chen, J. H.; Dorhout, P. K. *Inorg. Chem.* **1995**, *34*, 5705−5706.
(29) Chen, J. H.; Dorhout, P. K.; Ostenson, J. E. *Inorg. Chem.* **1996**, *35*, 5627−5633.
(30) Chondroudis, K.; Kanatzidis, M. G. *Inorg. Chem. Commun.* **1998**, *1*, 55−57.
(31) Chondroudis, K.; Kanatzidis, M. G. *Inorg. Chem.* **1998**, *37*, 3792−3797.
(32) Gauthier, G.; Jobic, S.; Brec, R.; Rouxel, J. *Inorg. Chem.* **1998**, *37*, 2332−2333.
(33) Aitken, J. A.; Chondroudis, K.; Young, V. G.; Kanatzidis, M. G. *Inorg. Chem.* **2000**, *39*, 1525−1533.
(34) Schleid, T.; Hartenbach, I.; Komm, T. *Z. Anorg. Allg. Chem.* **2002**, *628*, 7−9.
(35) Gauthier, G.; Evain, M.; Jobic, S.; Brec, R. *Solid State Sci.* **2002**, *4*, 1361−1366.
(36) Komm, T.; Schleid, T. *J. Solid State Chem.* **2005**, *178*, 454−463.
(37) Aitken, J. A.; Kanatzidis, M. G. *J. Am. Chem. Soc.* **2004**, *126*, 11780−11781.
(38) Komm, T.; Schleid, T. *Z. Anorg. Allg. Chem.* **2004**, *630*, 712−716.
(39) Komm, T.; Schleid, T. *J. Alloys Compd.* **2006**, *418*, 106−110.
(40) McGuire, M. A.; Reynolds, T. K.; DiSalvo, F. J. *Chem. Mater.* **2005**, *17*, 2875−2884.
(41) Gauthier, G.; Jobic, S.; Danaire, V.; Brec, R.; Evain, M. *Acta Crystallogr, Sect. C* **2000**, *56*, E117−E117.
(42) Goh, E. Y.; Kim, E. J.; Kim, S. J. *J. Solid State Chem.* **2001**, *160*, 195−204.
(43) Evenson, C. R.; Dorhout, P. K. *Inorg. Chem.* **2001**, *40*, 2884−2891.
(44) Evenson, C. R.; Dorhout, P. K. *Inorg. Chem.* **2001**, *40*, 2875−2883.
(45) Chan, B. C.; Hess, R. F.; Feng, P. L.; Abney, K. D.; Dorhout, P. K. *Inorg. Chem.* **2005**, *44*, 2106−2113.
(46) Hess, R. F.; Gordon, P. L.; Tait, C. D.; Abney, K. D.; Dorhout, P. K. *J. Am. Chem. Soc.* **2002**, *124*, 1327−1333.
(47) Hess, R. F.; Abney, K. D.; Burris, J. L.; Hochheimer, H. D.; Dorhout, P. K. *Inorg. Chem.* **2001**, *40*, 2851−2859.
(48) Liao, J. H.; Varotsis, C.; Kanatzidis, M. G. *Inorg. Chem.* **1993**, *32*, 2453−2462.
(49) Marking, G. A.; Evain, M.; Petricek, V.; Kanatzidis, M. G. *J. Solid State Chem.* **1998**, *141*, 17−28.
(50) Sheldrick, W. S. *Z. Anorg. Allg. Chem.* **1988**, *562*, 23−30.
(51) Belkyal, I.; El Azhari, M.; Wu, Y. D.; Bensch, W.; Hesse, K. F.; Depmeier, W. *Solid State Sci.* **2006**, *8*, 59−63.
(52) Wang, Z.; Willett, R. D.; Laitinen, R. A.; Cleary, D. A. *Chem. Mater.* **1995**, *7*, 856−858.
(53) Vysochanskii, Y. M.; Gurzan, M. I.; Maior, M. M.; Rogach, E. D.; Savenko, F. I.; Slivka, V. Y. *Kristallografiya* **1990**, *35*, 784−786.
(54) Maior, M. M.; Vysochanskii, Y. M.; Prits, I. P.; Molnar, S. B.; Slivka, V. Y.; Rogach, E. D.; Savenko, F. I.; Kudinov, A. P. *Inorg. Mater.* **1991**, *27*, 504−506.
(55) Arnautova, E.; Kosonogov, N.; Rogach, E.; Pavlov, A.; Protsenko, N.; Grekov, A. *Mater. Res. Soc. Symp. P* **1995**, *361*, 203−208.
(56) Bogomolov, A. A.; Malyshkina, O. V.; Solnyshkin, A. V.; Raevsky, I. P.; Protsenko, N. P.; Sandiev, D. N. *Izv. Akad. Nauk. Fiz.* **1997**, *61*, 375−378.
(57) Vysocahskii, Y. M.; Gurzan, M. I.; Maior, M. M.; Motrya, S. F.; Perechinskii, S. I.; Potorii, M. V.; Salo, L. A.; Khoma, M. M.; Slivka, V. Y.; Voroshilov, Y. V. *Sov. Phys. Solid State* **1985**, *27*, 525.
(58) Vlokh, R. O.; Vysochanskii, Y. M.; Grabar, A. A.; V., K. A.; Slivka, V. Y. *Izv. Akad. Nauk. SSSR, Neorg. Mater.* **1991**, *27*, 689−691.
(59) Gakh, S. G.; Litvinenko, V. Y.; Shneider, E. Y.; Borodin, V. Z. *Segnetoelektriki-poluprovodniki* **1986**, *4*, 83−87.
(60) Vlokh, R. O.; Vysochanskii, Y. M.; Grabar, A. A.; Kityk, A. V.; Slivka, V. Y. *Inorg. Mater.* **1991**, *27*, 570−572.
(61) Vysochanskii, Y. M.; Gurzan, M. I.; Maior, M. M.; Motrya, S. F.; Perechinskii, S. I.; Potorii, M. V.; Salo, L. A.; Khoma, M. M.; Slivka, V. Y.; Voroshilov, Y. V. *Fiz. Tverd. Tela.* **1985**, *27*, 858−864.
(62) Cleary, D. A.; Willett, R. D.; Ghebremichael, F.; Kuzyk, M. G. *Solid State Commun.* **1993**, *88*, 39−41.
(63) Liao, J. H.; Kanatzidis, M. G. *Inorg. Chem.* **1992**, *31*, 431−439.

(64) Schewe-Miller, I. *Metallreiche Hauptgruppenmetall-Chalkogen-Verbindungen: Synthese, Strukturen und Eigenschaften*; Max-Planck-Institut fur Festkorperforschung: Stuttgart, Germany, 1990.
(65) Kotiim, G. *Reflectance spectroscopy*; Springer-Verlag: New York, 1969.
(66) Wendlandt, W. W.; Hecht, H. G. *Reflectance Spectroscopy*; Interscience Publishers: New York, 1966.
(67) (a) Tandon, S. P.; Gupta, J. P. *Phys. Status Solidi* **1970**, *38*, 363−367. (b) McCarthy, T. J.; Kanatzidis, M. G. *Inorg. Chem.* **1995**, *34*, 1257. (c) Liao, J. H.; Kanatzidis, M. G. *Chem. Mater.* **1993**, *5*, 1561.
(68) *X-AREA*; STOE & Cie GmbH, IPDS Software: Darmstadt, Germany, 2006.
(69) Sheldrick, G. M. *SHELXTL*, Version 6.14; Bruker Analytical X-Ray Instruments, Inc.: Madison, WI, 2003.
(70) Sheldrick, G. M. *SADABS*; University of Göttingen: Göttingen, Germany, 2008.
(71) Petricek, V.; Dusek, M.; Palatinus, L. *Jana2006. Structure Determination Software Programs*; Praha, Czech Republic, 2006.
(72) Chupas, P. J.; Qiu, X. Y.; Hanson, J. C.; Lee, P. L.; Grey, C. P.; Billinge, S. J. L. *J. Appl. Crystallogr.* **2003**, *36*, 1342−1347.
(73) Hammersley, A. P.; Svensson, S. O.; Hanfland, M.; Fitch, A. N.; Hausermann, D. *High Pressure Res.* **1996**, *14*, 235−248.
(74) Egami, T.; Billinge, S. J. L. *Underneath the Bragg peaks: structural analysis of complex materials*; Pergamon Press: Oxford, England, 2003.
(75) Qiu, X.; Thompson, J. W.; Billinge, S. J. L. *J. Appl. Crystallogr.* **2004**, *37*, 678.
(76) Farrow, C. L.; Juhas, P.; Liu, J. W.; Bryndin, D.; Bozin, E. S.; Bloch, J.; Proffen, T.; Billinge, S. J. L. *J. Phys.: Condens. Matter* **2007**, *19*, 335219.
(77) Olbert, D.; Kalisch, A.; Gorls, H.; Ondik, I. M.; Reiher, M.; Westerhausen, M. *Z. Anorg. Allg. Chem.* **2009**, *635*, 462−470.
(78) Eichler, B. E.; Phillips, A. D.; Power, P. P. *Organometallics* **2003**, *22*, 5423−5426.
(79) Eichler, B. E.; Pu, L. H.; Stender, M.; Power, P. P. *Polyhedron* **2001**, *20*, 551−556.
(80) Elder, S. H.; Vanderlee, A.; Brec, R.; Canadell, E. *J. Solid State Chem.* **1995**, *116*, 107−112.
(81) Sourisseau, C.; Cavagnat, R.; Fouassier, M.; Brec, R.; Elder, S. H. *Chem. Phys.* **1995**, *195*, 351−369.
(82) Chondroudis, K.; Kanatzidis, M. G.; Sayettat, J.; Jobic, S.; Brec, R. *Inorg. Chem.* **1997**, *36*, 5859−5868.
(83) Becker, R.; Brockner, W.; Eisenmann, B. *Z. Naturforsch. A* **1987**, *42*, 1309−1312.
(84) Belkyal, I.; El Azhari, M.; Bensch, W.; Depmeier, W. *Acta Crystallogr., Sect. E* **2006**, *62*, I210−I212.
(85) Dittmar, G.; Schafer, H. *Z. Naturforsch. B* **1974**, *B 29*, 312−317.
(86) Gave, M. A.; Weliky, D. P.; Kanatzidis, M. G. *Inorg. Chem.* **2007**, *46*, 11063−11074.
(87) Arutyunyan, N. M.; Margaryan, A. A.; Khalilev, V. D. *Mater. Resp. Soveshch. Neorg. Khim.* **1976**, 57−59.
(88) Chiga, M.; Nakagawa, M., *Jpn. Kokai Tokkyo Koho* **2008**.
(89) Hayashi, A.; Yoshizawa, M.; Angell, C. A.; Mizuno, F.; Minami, T.; Tatsumisago, M. *Electrochem. Solid State* **2003**, *6*, E19−E22.
(90) Salmon, P. S.; Xin, S.; Fischer, H. E. *Phys. Rev. B* **1998**, *58*, 6115−6123.
(91) Ravaine, D. *J. Non-Cryst. Solids* **1980**, *38*−*9*, 353−358.
(92) Greiner, R.; Kapitza, H.; Ochsenkuehn, M. *Ger. Offen.* **2001**, 6.
(93) Greiner, R.; Kapitza, H.; Ochsenkuehn, M. *Ger. Offen.* **2001**, 4.
(94) Sistla, R. K.; Seshasayee, M. *J. Non-Cryst. Solids* **2004**, *349*, 54−59.
(95) Eckert, H.; Zhang, Z. M.; Kennedy, J. H. *Chem. Mater.* **1990**, *2*, 273−279.
(96) Kennedy, J. H.; Zhang, Z. M. *Solid State Ionics* **1988**, *28*, 726−728.
(97) Shibutani, Y.; Mizuno, F.; Hayashi, A.; Tatsumisago, M. *Khim. Inter. Ustoich. Razv.* **2007**, *15*, 219−223.
(98) Dhingra, S.; Kanatzidis, M. G. *Science* **1992**, *258*, 1769−1772.
(99) Kyratsi, T.; Chrissafis, K.; Wachter, J.; Paraskevopoulos, K. M.; Kanatzidis, M. G. *Adv. Mater.* **2003**, *15*, 1428−1431.
(100) Warren, B. E. *X-ray diffraction*; Dover: New York, 1990.
(101) Yamada, N.; Ohno, E.; Nishiuchi, K.; Akahira, N.; Takao, M. *J. Appl. Phys.* **1991**, *69*, 2849−2856.
(102) Rubin, K. A.; Birnie, D. P.; Chen, M. *J. Appl. Phys.* **1992**, *71*, 3680−3687.
(103) Ohta, T. *J. Optoelectron. Adv. Mater.* **2001**, *3*, 609−626.
(104) Yamada, N.; Matsunaga, T. *J. Appl. Phys.* **2000**, *88*, 7020−7028.
(105) Chrissafis, K.; Kyratsi, T.; Paraskevopoulos, K. M.; Kanatzidis, M. G. *Chem. Mater.* **2004**, *16*, 1932−1937.